Available online at www.sciencedirect.com

ScienceDirect

Energy Procedia 57 (2014) 570 – 579

Energy Procedia

2013 ISES Solar World Congress

Heat transfer modeling and analysis of solar thermo-chemical reactor for hydrogen production from water

K. S. Reddy*, Premkumar. D, T. Srihari Vikram

Heat Transfer and Thermal Power Engineering, Department of Mechanical Engineering, Indian Institute of Technology Madras, Chennai – 600036, India

Abstract

A solar thermo-chemical reactor is modeled and analyzed for the solar thermal dissociation of zinc oxide into zinc and oxygen involved in the thermo-chemical cycle for hydrogen production. The reactor consists of a cavity surrounded by a rotating insulation layer made of alumina. The granular zinc oxide particles are fed into the cavity and are directly exposed to the solar radiation entering the cavity through a quartz window. A three dimensional numerical model coupling the multiphase particle dynamics in gravitational field, multiphase heat transfer, k-ε turbulence model, discrete ordinates radiation model, Arrhenius reaction rate model is developed. The cavity temperature and oxygen molar flow rate at the outlet of the reactor which is the indicator of the reaction rate has been validated with a 10kW reactor prototype. An energy balance study of thermal performance parameters including the various losses occurring from the reactor and efficiency is also done. The major losses were contributed by re-radiation (46%) and sensible heating of reactor components (35.5%), while the minor losses were contributed by convection by argon (1%) and conduction through insulation (2%).The thermal efficiency of the reactor is calculated to be 15.5%.

Selection and/or peer-review under responsibility of ISES.

Keywords: Heat transfer modeling; solar thermo-chemical reactor, hydrogen production

1. Introduction

Hydrogen is a clean-burning fuel and when combined with oxygen in a fuel cell, it produces heat and electricity with only water vapor as by-product. However, hydrogen does not exist freely in nature; it is

* Corresponding author. Tel.+91-44-22574702; fax: +91-44-22574652.
E-mail address: ksreddy@iitm.ac.in (K. S. Reddy)

Selection and/or peer-review under responsibility of ISES.
doi:10.1016/j.egypro.2014.10.211

Nomenclature

A_p	pre-exponential factor of Arrhenius reaction rate model
d	diameter of granular particles (m)
e_{ss}	restitution coefficient
E	activation energy (kJ/mol)
$\vec{g}$	gravitational acceleration vector (m/s^2)
$g_{0,ss}$	radial distribution function
h	enthalpy (J/kg)
h_{pq}	heat transfer coefficient between primary and secondary phase (W/m^{2}K)
$K_{l,s}$	momentum exchange coefficient
k	thermal conductivity (W/mK)
M_w	molecular weight (kg/kmol)
p	absolute pressure (N/m^2)
R	universal gas constant (J/K-mol)
r	radial coordinate
r_{ZnO}	rate of Zinc oxide dissociation reaction
S_{pq}	energy source/sink due to radiation and chemical reaction
s	mass source/sink due to chemical reaction (kg)
T	temperature (K)
t	flow time (s)
$\vec{v}$	velocity vector (m/s)
z	axial coordinate

Greek symbols

α	volume fraction
μ	dynamic viscosity (Pa.s)
$\mu_{s,\,col}$	collisional part of granular shear viscosity (Pa.s)
$\mu_{s,\,kin}$	kinetic part of granular shear viscosity (Pa.s)
ρ	density (kg/m^3)
$\bar{\bar{\tau}}$	stress tensor
Θ	granular temperature (K)

produced from other sources of energy, so it is often referred as an energy carrier unlike a primary energy source like coal. Hydrogen is an efficient way to store and transport a huge amount of energy since it has a high calorific value than any fossil fuel. Solar thermo-chemical methods, one of the methods to produce hydrogen are based on the cyclic process of reduction and oxidation of metal oxides and metals respectively. The hydrogen and oxygen are by-products of the reaction. Several two-step water-splitting cycles based on metal oxide redox reactions including ZnO/Zn, TiO_2/TiOx, Mn_3O_4/MnO and Co_3O_4/CoO have been proposed. But the cycle based on Zn/ZnO redox reactions [1] has much higher practical hydrogen yield and operates at a moderate temperature compared to ferric and ceria cycles except carbothermal reduction of ZnO.

The ZnO produced is used again for the dissociation process, thus completing the two step cycle. The separation of zinc vapor and oxygen in the first step is accomplished by quenching the gas mixture in an inert atmosphere of argon gas. The exergy efficiency for a 10 kW reactor has a maximum value of 29% without any heat recovery but the theoretical maximum with heat recovery during quenching and hydrolysis is 82% [2]. The first step of the cycle is performed in a direct incident solar thermo-chemical reactor. The process occurs in a rotating cavity receiver lined with ZnO particles held to the cavity wall by centrifugal action while exposing the particles to highly concentrated solar radiation.

The objective of this work is to numerically model the solar thermo-chemical reactor coupling the granular particle physics, radiation modelling, and chemical reaction modelling using a finite volume based CFD package and to simulate the various processes occurring within the reactor.

1.1 Solar thermo-chemical reactor

The solar reactor configuration consists of 160 mm diameter rotating cylindrical cavity which is composed of sintered ZnO tiles glued on sintered alumina insulation [3]. The ZnO tiles serve as shock absorber and thermal insulator. The cavity wall is further surrounded by a layer of insulating alumina fibers whose density is much lesser than sintered alumina thus reducing the sensible heat loss. Concentrated solar radiation enters the cavity through a quartz window which is mounted on a conical frustum attached to the cavity of the reactor. The radiation further enters the cavity through a 30 mm diameter aperture. Preheated argon quench gas at 1000 K is injected through 6 nozzles placed symmetrically around the conical wall at a mass flow rate of 0.02 g/s through each nozzle.

2. Modeling of reactor for solar hydrogen production

2.1 Physical model and design of solar thermo-chemical reactor

The solar reactor consists of multiphase zone, sintered alumina solid zone and an insulation solid zone as shown in Fig 1. The length of the cavity of the reactor is 230 mm while the cavity diameter is 160 mm. Argon quench gas is injected into the cavity through six jets placed symmetrically around the cavity. The wall of the cavity is made up of 2 mm thick ZnO tiles. The cavity wall is surrounded by a layer of sintered alumina of thickness 4mm which act as thermal shock absorber and to some extent as thermal insulator. The next insulation layer made up of 110 mm thick alumina fibers surrounds the sintered alumina layer. In order to prevent hot gases escaping from reactor cavity through the aperture and to reduce re-radiation losses, a 3 mm thick quartz window is mounted on a water-cooled aluminum ring and integrated to the front face of cavity via conical frustum. Concentrated solar radiation from the parabolic dish at flux intensity of about 5000 suns enters the cavity through quartz window. The reactor has a dynamic feeder that extends and retracts within the cavity and enables to evenly spread out a layer of ZnO particles of desired thickness along the entire cavity.

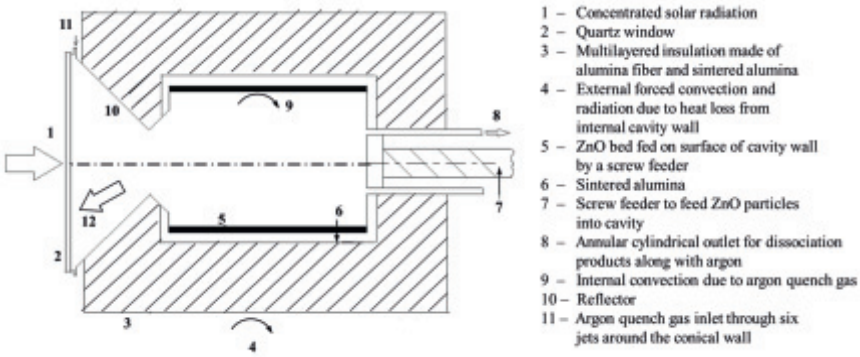

Fig.1. Physical model of solar thermo-chemical reactor

2.2 Methodology of heat transfer analysis of the reactor

The solar thermo-chemical reactor has been modelled and simulated using the finite volume based CFD package ANSYS Fluent [4]. The geometry of the reactor has been created using CATIA. The coupled phenomenon of fluid flow of gaseous mixture, multiphase particle physics of ZnO particles, turbulence, radiation physics and chemical reaction for ZnO dissociation has been included in the model. CFD analysis has been performed on a 3-D reactor domain consisting of cavity, sintered alumina and insulation made of alumina fibers. The mesh of the solid part of reactor domain is assumed to be rotating at 120 rpm in order to keep the ZnO particles along the wall by centrifugal action.

The particle dynamics of ZnO particles has been modelled by Eulerian-Eulerian multiphase model to find the radial and axial distribution of volume fraction of ZnO particles inside the cavity. This methodology gives a more accurate prediction of the reaction rate because of the correct volume fraction distribution spatially. The gaseous phase consisting of argon, zinc (g) and oxygen is assumed to be primary phase while the granular ZnO particles is assumed to be secondary phase. Separate continuity, momentum, energy equations has been solved for each phase. The mean particle size is assumed to be 10 microns. The turbulence phenomenon of both the phases is captured separately by k-ε turbulence model. Standard wall functions were used to capture the boundary layer effects of the rotating cavity wall. RNG k-ε model is considered to account for swirl dominated flow features to accurately predict the viscous effects between the particles and the gaseous phase. Discrete Ordinates radiation model is used to describe the radiation phenomenon occurring within the reactor. The number of azimuthal and zenith divisions considered were 4 per octant therefore the radiation intensity was calculated in a total of 128 directions per finite volume cell. The flux distribution at the quartz window is assumed to be of Gaussian distribution with a radial standard deviation of 5 mm and the maximum value varying with time. The cavity walls are assumed to be completely diffuse emitters of radiation.

The dissociation of ZnO(s) into zinc(g) and oxygen is a case of heterogeneous phase reaction where the reaction rate follows Arrhenius reaction rate model. The activation energy and pre-exponential factor [7] for the reaction are considered as 361 kJ/mol.K and 14 x 10^6 kg/m^2s. In order to consider the solid and gaseous phase separately two mixture materials created. The gaseous mixture is a combination of zinc, oxygen and argon while the solid mixture consists of only granular ZnO particles. The thermo physical properties of gases like thermal conductivity, viscosity and mass diffusivity are considered as a function of temperature and follow kinetic theory.

2.3 Governing equations

The continuity equation for any general phase 'q' is given by [5],

$$\frac{\partial}{\partial t}\left(\alpha_q \rho_q\right)+\nabla.\left(\alpha_q \rho_q \overrightarrow{v_q}\right)=S_q \tag{1}$$

The momentum equation for any phase 'q' is given by [5],

$$\frac{\partial}{\partial t}\left(\alpha_q \rho_q \overrightarrow{v_q}\right)+\nabla.\left(\alpha_q \rho_q \overrightarrow{v_q}\overrightarrow{v_q}\right)=-\alpha_q \nabla p+\nabla.\overline{\overline{\tau_q}}+\alpha_q \rho_q \vec{g}+K_{ls}\left(\overrightarrow{v_l}-\overrightarrow{v_s}\right) \tag{2}$$

The kinetic viscosity between the granular particles [5] is a sum of collisional and kinetic components. The collisional viscosity is given by,

$$\mu_{s,col}=\frac{4}{5}\alpha_s \rho_s d_s g_{0,ss}\left(1+e_{ss}\right)\left(\frac{\Theta_s}{\pi}\right)^{1/2}\alpha_s \tag{3}$$

The kinematic viscosity between the granular particles is given by [5],

$$\mu_{s,kin}=\frac{10\rho_s d_s\sqrt{\Theta_s \pi}}{96\alpha_s\left(1+e_{ss}\right)g_{0,ss}}\left[1+\frac{4}{5}\alpha_s\left(1+e_{ss}\right)g_{0,ss}\right]^2\alpha_s \tag{4}$$

During the phase change from solid to gas the momentum of the solid is transferred to the gaseous medium.

The energy equation for any phase 'q' is given by [5],

$$\frac{\partial}{\partial t}\left(\alpha_q \rho_q h_q\right)+\nabla.\left(\alpha_q \rho_q \overrightarrow{v_q} h_q\right)=-\alpha_q \frac{\partial p_q}{\partial t}+\overline{\overline{\tau_q}}\nabla\overrightarrow{v_q}+S_{hq}+Q_{pq} \tag{5}$$

where $Q_{pq}=h_{pq}(T_p-T_q)$ and $h_{pq}=(6\kappa_q\alpha_p\alpha_q Nu_p)/d_p^2$

The Nusselt number was represented as a complex function of volume fraction, Reynolds number, Prandtl number [6]. The heterogeneous reaction rate reaction rate governed by Arrhenius reaction rate model is given by [7],

$$k=A_p e^{\left(\frac{-E}{RT}\right)} \tag{6}$$

2.4 Boundary conditions

The various boundary conditions are given below:

(1) Argon injection through six nozzles is modeled as *mass flow inlet* boundary condition with a mass flow rate of 0.02 g/s through each nozzle entering at 1000K.
(2) Outlet of reactor is modeled as *pressure outlet* at absolute pressure of 1 atm.
(3) The inner cavity wall which is rotating at 120 rpm has a wall roughness height of 0.01 mm and an emissivity of 0.7.
(4) Energy loss from the aluminum outer wall is considered as *mixed wall* boundary condition combining radiation and convection to the ambient at 300 K.
(5) For the rotating outer cylindrical shell, heat transfer coefficient [8] is h = 6.2 W/m^2K.
(6) For the front and back portion of outer wall including quartz window, heat transfer coefficient [9] is h = 23W/m^2K.

(7) The window of the reactor is modeled as a semi-transparent wall made of quartz glass with transmissivity of 0.9. The input beam radiation at the window is time and space variant. The flux distribution at the aperture as a function of radial coordinate and is represented as a two dimensional Gaussian distribution function

$$F(r,z) = A\exp\left(-\frac{1}{2}\left[\left(\frac{r-\mu}{\sigma_r}\right)^2+\left(\frac{z}{\sigma_z}\right)^2\right]\right) \quad (7)$$

Where $\mu = \sqrt{\frac{2}{\pi}}z$ and σ_r =5mm; $\sigma_z = 4\sigma_r$

3. Results and discussion

3.1Model validation

The heat transfer model is validated with the experimental data [3] considering the cavity temperature and oxygen molar flow rate through the outlet. The experiments have been carried using high-flux solar simulator at Paul Scherrer Institute, Switzerland. The cavity temperature has been measured using Type-B thermocouples at the back of ZnO tiles. The oxygen molar flow rate through the outlet is one of the indicators of the progress of the reaction. The model cavity temperature was slightly higher than that of the experimental value by 10 K as shown in Fig. 2 (a). The oxygen molar flow rate varied with time in a smooth manner as opposed to the transient fluctuations in case of experimental run due to noise in measurement as shown in Fig. 2 (b). The drop in oxygen flow rate at 3400 s is due to the formation of CO_2 due to the oxidation of carbon impurities present in the ZnO feed. At lower temperatures i.e, 1500-1700 K the deviation from the experimental value is not substantial but at higher temperatures the deviation is high which indicates the dependence of the reaction pre-exponential factor on temperature.

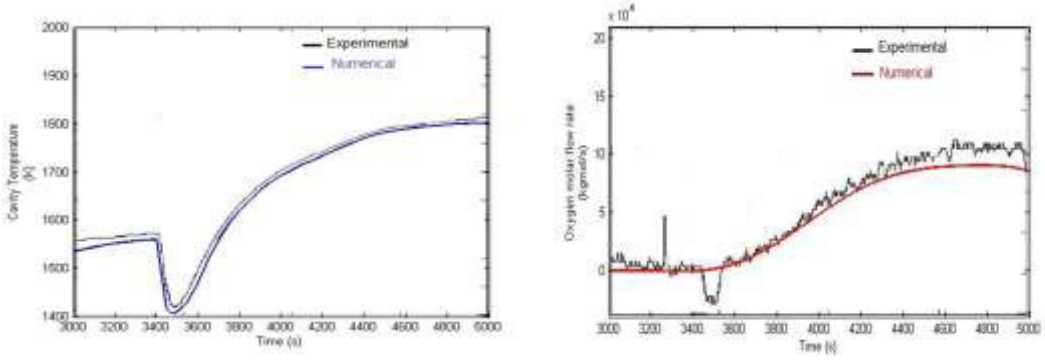

(a) (b)

Fig. 2. Validation of model with experimental data (a) cavity temperature and (b) oxygen molar flow rate

3.2 Sensible heating of reactor

The dissociation of ZnO in a thermochemical reactor at various stages is shown in Fig. 3 (a). The first phase starts with gradual sensible heating of reactor components such as the cavity wall and multilayered insulation. During the second phase, reactor heating is stopped and the screw feeder is extended into the reactor cavity in order to feed the granular ZnO particles uniformly over the cavity wall. At the end of feeding the screw feeder is retracted and the power input is fixed to a constant maximum

value. During this phase, as the temperature of ZnO particles increases the dissociation process and proceeds at a faster rate until the entire ZnO mass is exhausted. During the initial heating phase, the reactor is gradually heated to 1560 K. The gradual heating results in lesser thermal expansion and therefore lesser stresses. The sensible heating is done by varying the input power through the aperture from 0 to 4 kW for about 3400 s as shown in Fig. 3 (a). The power input is assumed to be proportional to the square root of flow time. The cavity temperature increases gradually and attains a maximum value of 1825 K at 5025s as shown in Fig. 3(b). The rate of rise of cavity temperature dropped with time due to the increase in reaction heat and re-radiation loss.

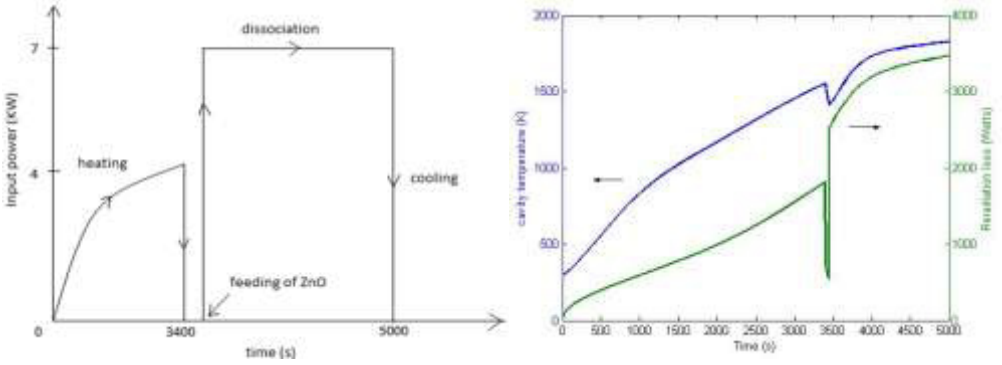

(a) (b)

Fig. 3 (a) Variation of power input with time (b) Variation of cavity temperature and re-radiation loss with time

From the start of heating to 1000 s, there is an increase in rate of temperature rise. The re-radiation loss which is proportional to the fourth power of cavity temperature, increases nonlinearly with temperature and hence results in reduction of sensible heating of the insulation. This results in reduction in the rate of rise of cavity temperature and hence after 1000 s, the temperature varies linearly with time. Fig. 4 shows the temperature contour at the end of heating and dissociation stages. The temperature of the inner cavity wall peaks at the center region and then falls of gradually which is due to the higher intensity

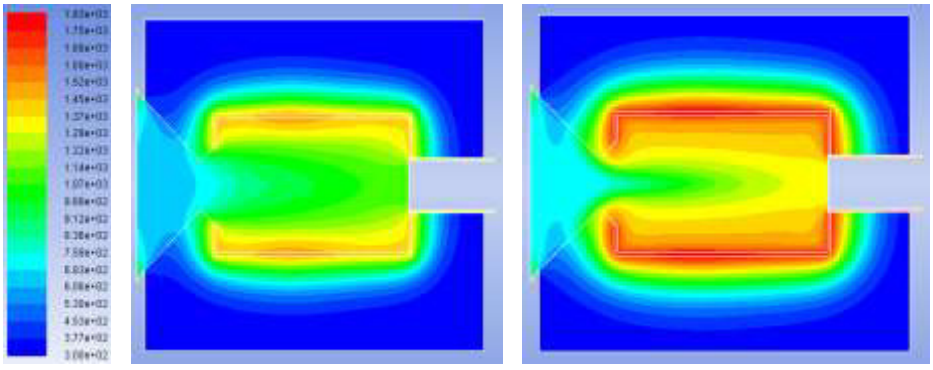

(a) (b)

Fig. 4. (a) Temperature (K) contours at the end of (a) heating phase at 3400 s (b) dissociation at 5000 s

of incident radiation as shown in Fig. 5 (a). The outer wall temperature did not change much from the initial temperature of 300 K and hence resulted in negligible conduction loss. The re-radiation loss contributes about 32% of the input energy while the maximum portion of 66% goes into sensible heating of the insulation. The rest of the input energy is lost by convection through argon quench gas and by

conduction through the insulation to the ambient at 300 K. Fig. 5 (b) shows the diffusion of momentum through the fluid domain due to the wall rotation. The argon quench gas attained a velocity of 0.1 m/s at the aperture. The cavity temperature dropped due to the absorption of the heat by the freshly fed ZnO particles and by re-radiation loss.

3.3 Feeding of zinc oxide

After the sensible heating of the reactor cavity and insulation, about 284 g of ZnO particles is fed for 50 s into the rotating reactor cavity. During the feeding phase, the input power is stopped so that the temperature does not rise which would otherwise increase the dissociation of ZnO. The momentum diffused through the fluid domain due to the wall rotation. The argon quench gas attained a velocity of 0.1 m/s at the aperture. The cavity temperature is dropped due to the absorption of the heat by the freshly fed ZnO particles and also by re-radiation loss. At the end of heating phase, the cavity temperature reached a maximum value of 1560 K. After 50 s of the feeding phase, cavity temperature dropped by 150 K. The dissociation reaction of ZnO based on Arrhenius model initiated and the products of reaction, i.e, zinc (g)

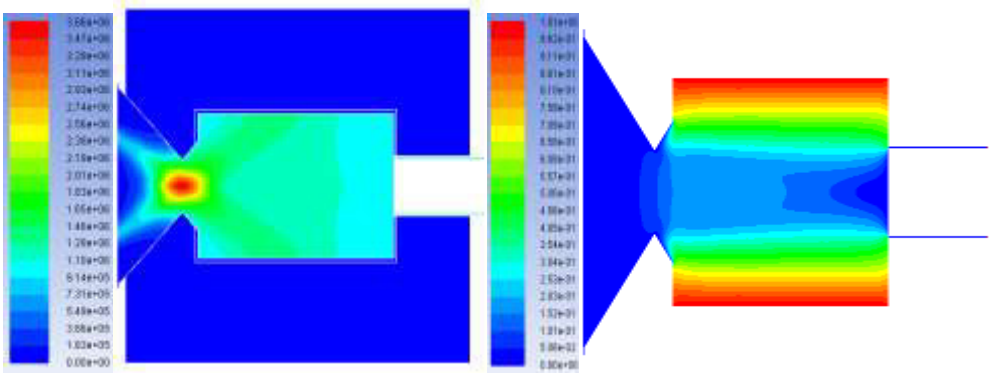

(a) (b)

Fig 5 Contours of (a) radiation flux (b) velocity

and oxygen started to form and the molar flow rate of the products increased following the trend of reaction rate. But, the maximum reaction rate did not exceed 0.004 g/s and the oxygen molar flow rate at the outlet reached a maximum of 1 x 10-7mol/s. A recirculation zone has been noticed near the aperture of the reactor inside the cylindrical cavity region due to the combined effect of axial flow and swirl flow. This resulted in flow reversal out of the reactor cavity through the aperture into the conical wall region. At the end of feeding phase, ZnO particles were distributed through 4 mm from the cavity wall. All the ZnO particles were within the created inflation boundary layer mesh.

3.4 Dissociation of zinc oxide

The third phase of the simulation is the important phase of reaction wherein the cavity temperature increases and results in an exponential increase in reaction rate. The input power is increased to a maximum value of 7 kW and kept constant. The oxygen molar flow rate initially increases exponentially with time, but after 4500 s due to the reduced rate of rise in temperature and concentration of particles, the reaction rate drops and hence the oxygen molar flow rate also drops. From the Fig. 6, it can be seen that at the end of the reaction, heat from the cavity wall diffused more through the insulation and hence increasing the outer wall loss by convection and radiation to the ambient. At the end of dissociation, the

maximum mass fraction of zinc is 0.68 and that of oxygen is 0.17 (Fig 6). The highest concentration of zinc and oxygen was near the ZnO bed and dropped gradually towards the axis of the reactor.

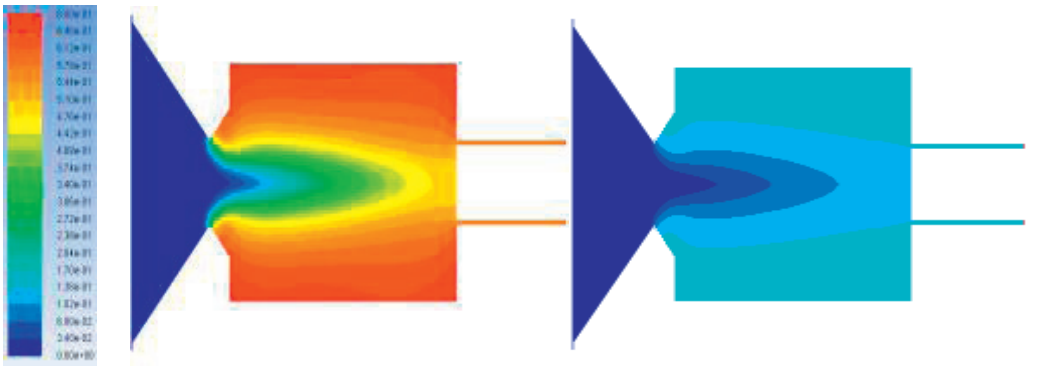

(a) (b)

Fig 6 Contours of mass fraction at 4700 s (a) zinc (b) oxygen

3.5 Energy balance and efficiency of the reactor

The maximum rate of heat addition through the aperture of the reactor is fixed at 7 kW. Various losses occurring in the reactor has been studied. The losses include re-radiation from the cavity, convective loss by argon quench gas, conductive losses from the insulation to ambient and sensible heating of insulation. From the analysis, it is found that the contribution of re-radiative loss is 46% of the total energy input while sensible heating of the insulation accounted for 35.5% of total energy input as shown in Fig 7 (a). Minor losses including the convective loss by argon quench gas and conductive loss to the losses contributed 1% and 2% respectively. The variation of heat losses with flow time occurring in the alumina reactor is shown in Fig. 7 (b). The rate of rise of re-radiation loss for the reactor is higher during the earlier stage of dissociation since re-radiation loss is a function of cavity temperature. But as the cavity temperature increases nonlinearly, the re-radiation loss also increases and the amount of energy heating the reactor insulation decreases. Hence the rate of temperature rise decreases and the temperature.

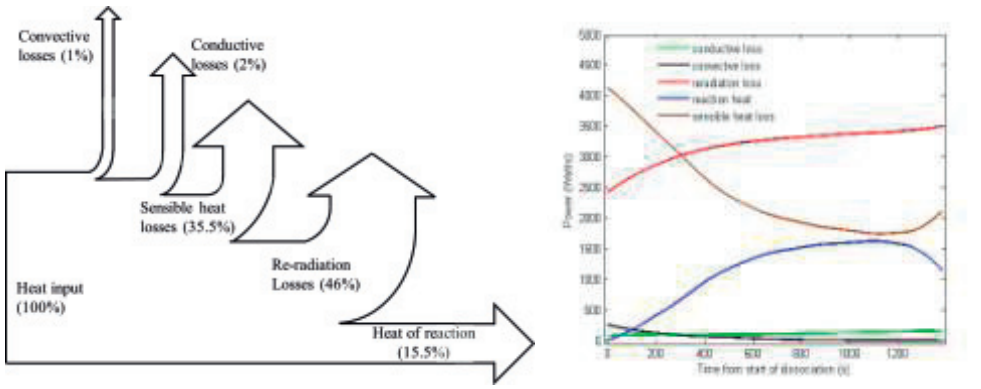

(a) (b)

Fig 7 (a) Energy balance of the reactor (b) Variation of heat losses with time

and re-radiation loss almost attains a constant value. The sensible heating of the reactor insulation is the most dominant form of heat loss at the start of dissociation phase, since the ZnO bed temperature is very less for the dissociation reaction to attain maturity. But as the cavity temperature increases, the reaction

rate is also increased following Arrhenius reaction rate model for heterogeneous media. Hence majority of input energy is utilised for energy required for dissociation of ZnO and the re-radiation loss. This results in a drop of sensible heat loss in the reactors

The mean reactor efficiency of the reactor is defined as ratio of useful energy of the reaction to the input energy and it is found out to be 15.5%. The useful energy is a sum of heat of reaction and sensible heat absorbed by ZnO particles.

The mean reactor efficiency is given by,

$$\eta_{th} = \frac{r_{ZnO}\left(\Delta H_r(T_r) + \int_{T_0}^{T_r} c_{p,ZnO}\,dT\right)}{q_{solar}} \tag{8}$$

4. Conclusions

A solar thermo-chemical reactor has been modelled and analyzed by coupling 3-D multiphase particle physics, discrete ordinates radiation model and Arrhenius reaction rate model. The cavity temperature and oxygen molar flow rate has been validated with experimental data. The deviation between the experimental and model data of oxygen molar flow rate increased at higher temperatures indicating the variation of pre-exponential factor of the reaction with temperature. Oxygen molar flow rate attained a maximum value of 8 x 10^{-6}mol/s at 4500 s. Energy balance analysis has been carried out on modelled reactor and the contribution of various losses were studied. Radiative and sensible losses contributed 46 % and 35.5% of the input radiative energy. The thermal efficiency of the reactor is calculated to be 15.5 %.

References

[1] Palumbo R, Lede J, Boutin O, Elorza-Ricart E, Steinfeld A, Moeller S, Weidenkaf A, Fletcher EA, Bielicki J. The production of Zn from ZnO in a single-step high temperature solar decomposition process; *Chem Eng Sci.* 1998; **53**: 2503-18.

[2] Steinfeld A. Solar thermo-chemical production of hydrogen–a review; *Sol. Energ.* 2005; **78**:603-615.

[3] Schunk LO, Haeberling P, Wepf S, Wuillemin D, Meier A, Steinfeld A. A receiver-reactor for the solar thermal dissociation of zinc oxide; *Sol. Energ. Eng.* 2008; **130**: 021009-6.

[4] ANSYS 2011 Inc., ANSYS FLUENT 14 Theory guide

[5] Gidaspow D, Bezburuah R, Ding J. Hydrodynamics of circulating fluidized beds: Kinetic theory approach; In: Fluidization VII, Proceedings of 7th Engineering Foundation Conference on Fluidization, 1992;75–82.

[6] Gunn DJ. Transfer of heat or mass to particles in fixed and fluidized beds; *Int. J. Heat Mass Transfer* 1978; **21**:467–476.

[7] Lothar OS, Steinfeld A. Kinetics of the thermal dissociation of ZnO exposed to concentrated solar irradiation using a solar-driven thermo-gravimeter in the 1800–2100 K Range; *AIChE* 2009; **55**: 1497 – 1504.

[8] Özerdem B, Measurement of convective heat transfer coefficient for a horizontal cylinder rotating in quiescent air; *Int. Commun. of Heat Mass Transfer* 2000; **27**: 389–395.

[9] Shieh YR, Li CJ, Hung YH. Heat transfer from a horizontal wafer-based disk of multi-chip modules; *Int. J. of Heat Mass Tran*. 1999; **42**: 1007–1022.